PCCP

RSC Publishing

PAPER

View Article Online
View Journal

Cite this: DOI: 10.1039/c3cp53902d

Structure & bonding of the gold-subhalide cluster *I*-$Au_{144}Cl_{60}^{[z]}$†

Alfredo Tlahuice-Flores,* David M. Black, Stephan B. H. Bach, Miguel Jose-Yacamán and Robert L. Whetten*

Received 30th July 2013,
Accepted 27th September 2013

DOI: 10.1039/c3cp53902d

www.rsc.org/pccp

The structure and bonding of the gold-subhalide compounds $Au_{144}Cl_{60}^{[z]}$ are related to those of the ubiquitous thiolated gold clusters, or Faradaurates, by iso-electronic substitution of thiolate by chloride. Exact *I*-symmetry holds for the [*z*] = [2+,4+] charge-states, in accordance with new electrospray mass spectrometry measurements and the predicted electron shell filling. The high symmetry facilitates analysis of the global structure as well as the bonding network, with some striking results.

Self-assembled monolayers (SAMs) of thiolates on noble-metal electrodes and nanostructures are regarded as prime examples of chemical nanotechnology,[1,2] based upon the bridging coordination of the thiolate-sulfur head-group,[3] as established only recently by rigorous structure determination.[4,5] Remaining challenges concern the complexity of the electronic structure and bonding that underlie the observed phases and their properties.

Here we consider the structure (Fig. 1) of the large gold-subchloride $Au_{144}Cl_{60}^{[2+/4+]}$ cluster, as an isoelectronic analog[6] of the ubiquitous thiolated gold clusters $Au_{144}(SR)_{60}^{[z]}$, also known as Faradaurates.[7,8] This construction is also of interest for its exceptionally high symmetry (*I*) and compactness [see below].

Fig. 2 provides evidence of a limiting charge-state [4+], present in the solution-phase of a sample (prepared using R = $-CH_2CH_2Ph$) beyond that which could be obtained in the pioneering ESI-MS measurements.[9–12]

The Fig. 2 inset presents an energy-level diagram, characteristic of *I*-$Au_{144}Cl_{60}^{[z]}$ as well as $Au_{144}(SR)_{60}^{[z]}$,[13] depicting the filling of the frontier orbitals for each state.

The structure of *I*-$Au_{144}Cl_{60}$ was obtained either by: (i) isoelectronic substitution[6] of chloride ions (Cl^-) for hydrogen-sulfide (HS^-) or methane-thiolate (CH_3S^-) anions, starting from the models[13] motivated by ref. 14; or (ii) *de novo* construction from the crystal structure of the icosahedral compound $Pd_{145}(CO)_{60}(PR_3)_{30}$.[15]

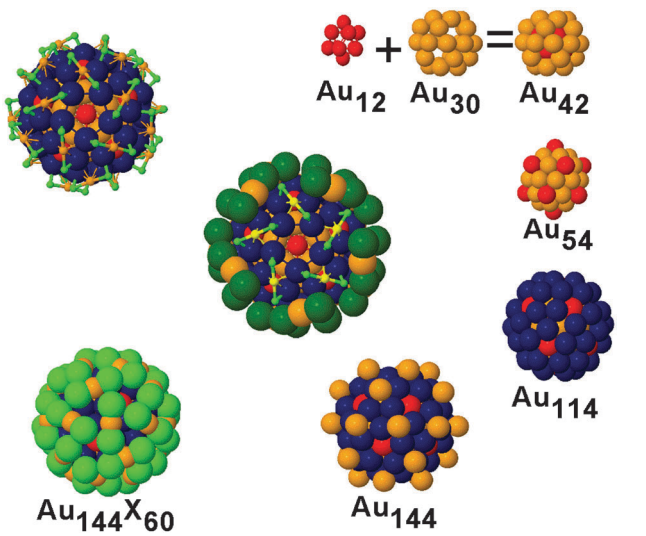

Fig. 1 Structure of the *I*-$Au_{144}X_{60}^{[z]}$ compound, clock-wise from top right: assembly of the 42-Au structure from the hollow inner 12-Au shell (red) and the inner 30-Au shell (orange). Adding the outer 12-Au (also red) yields the 'inner core' comprising 54-Au atoms. The 'grand core' view Au_{114} highlights the shell of 60-Au sites (blue) in relation to the outer 12-Au sites. The Au_{144} substructure (bottom center) adds 30-Au sites (also orange). The 60-X halide sites (green) complete the assembly (lower left) and define its topography. The view at top left, along a C_5 symmetry axis, exposes the symmetric arrangement of 'staple-motif' surface units. At centre, the cutaway view of the spacefilling C_5 perspective highlights five of the staple units (in small light green for Cl and small yellow for Au). Color code: 60-X = green; outer 30-Au = small orange; 60 Au = blue; groups of 12 Au = red; inner 30-Au = orange.

In both cases, the same structure is obtained *via* energy minimization based upon density functional theory (DFT) electronic structure calculations. The *I*-$Au_{144}Cl_{60}^{[z]}$ structures are then re-optimized for each charge-state [*z*] considered. The methods were tested by repeating the recent analysis of T_h-$Au_{25}Cl_{18}^{[1-]}$ by Jiang and Walter.[6]

Departments of Physics & Astronomy and Chemistry, University of Texas, San Antonio, TX, 78249, USA. E-mail: tlahuicef@gmail.com, Robert.Whetten@utsa.edu

† Electronic supplementary information (ESI) available: Experimental methods and materials; theoretical method and tables and graphs including the structure analysis of various $Au_{144}R_{60}^{[z]}$ clusters. See DOI: 10.1039/c3cp53902d

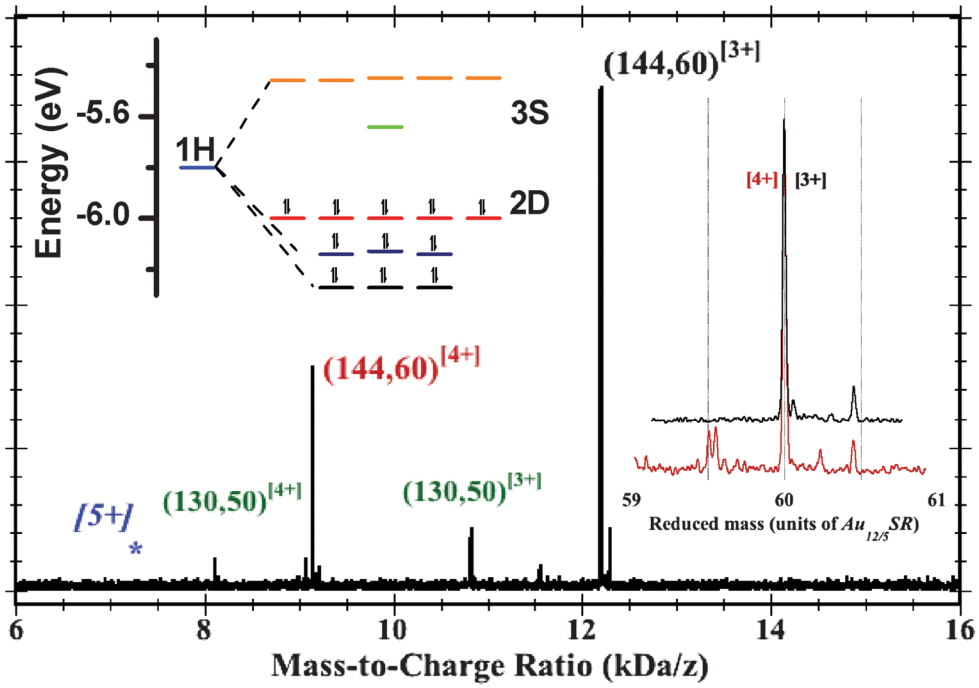

Fig. 2 Mass spectrum of a sample of purified $Au_{144}(peth)_{60}$ clusters, obtained by the electrospray-ionization time-of-flight method. [See ESI,† section.] The labelled peaks indicate the assignments to the [3+] (black) and [4+] (red) charge-states. The blue [5+] and asterisk indicate the expected location of the missing [5+] peak near 7.2 kDa per z, and the green-labeled peaks designate a residual impurity (or byproduct) also known from earlier research. Right inset: expanded regions of the [4+] and [3+] peaks, plotted *versus* the mass (rather than mass-to-charge ratio), in units of the 60-fold unit (~0.610 kDa) of $Au_{12/5}(peth)_1$, so that the principal peaks are overlaid at reduced-mass 60. The position and width (FWHM ~ 12 Da) of these peaks are consistent with the natural isotope abundance of ^{13}C. Minor satellite peaks toward higher masses are assigned to Cs^+-adduct formation (each Cs-atom is 0.133 kDa, or 0.218 on the reduced-mass scale). The main satellite peak toward lower mass is attributed to organic disulfide (RS–SR) loss (0.274 kDa, or 0.448). Left inset: energy-level diagram for the frontier orbitals of $Au_{144}Cl_{60}^{[4+]}$ (HOMOs $2D^{10}$, LUMO $3S^0$) but generic to the I-$Au_{144}(SR)_{60}^{[z+]}$ systems. Seventeen (17) orbitals are classified according to united-atom (or 'superatom')[27] representations {1H, 2D, 3S}, where {S,P,D,F,G,H, ...} denote respective total angular momenta L = {0,1,2,3,4,5, ...} with $(2L + 1)$-fold orbital degeneracy. The electronic 1H-shell splits under an icosahedral field into groups of (3,3,5) each, *cf.* I_h-C_{60} or -C_{80} clusters.[19] Electronic closed-shell configurations are thus predicted for charge-states [4+] (depicted), [2+], and [8−]. The neutral state is open shell and subject to Jahn–Teller instability (deformation); see ESI,† for details.

We assessed the cohesion of this structure by the following chemical equation, representing decomposition of I-$Au_{144}X_{60}$ into 'super-stable' closed-shell I-Au_{72} and $[Au(I)X]_4$ 'rings'.[6,16]

$$I\text{-}Au_{144}X_{60} \rightarrow (7/6)\ I\text{-}Au_{72} + 15\ [Au(I)X]_4$$

The energy required is +68 eV, which is +110 kJ mol^{-1}-Cl (+45 kJ mol^{-1}-Au). Thus the structure is highly cohesive.

The optimized structure holds chiral-icosahedral (I) symmetry, at a tolerance of 0.13 Å in the neutral [z = 0] state, improving to 0.03 Å in both [2+] and [4+] states. These reflect

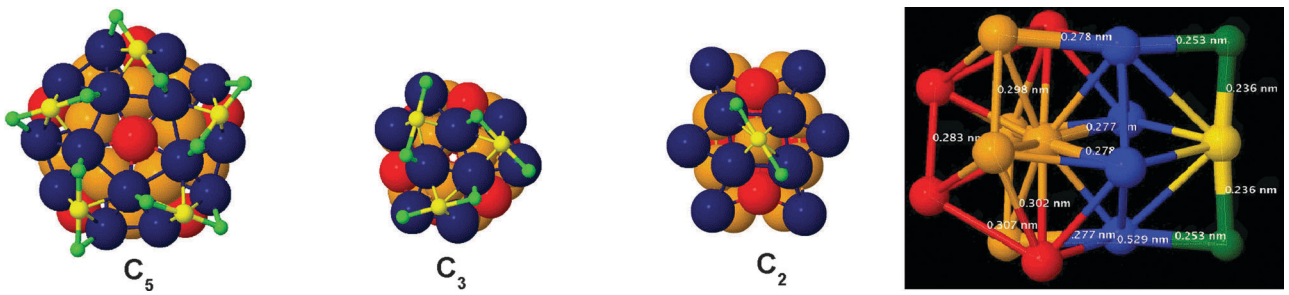

Fig. 3 Sections of the structure of I-$Au_{144}Cl_{60}^{[2+]}$. The repeated surface-structure and bonding of the I-$Au_{144}Cl_{60}$ structure are illustrated by views along one each of the {6 C_5, 10 C_3, 30 C_2} symmetry axes, corresponding to orthogonal projections of the I-symmetry polyhedron ($3^4.5^*$).[20] The colour scheme is preserved from Fig. 1. Left: the C_5-projection, *cf.* Fig. 1, shows the mutual orientations among five staple-motif units, revealing a chiral 'Texas-Star' pattern. Center-left: the C_3-projection centers on a hole, and shows the mutual orientations of three staple-motif units. Center-right: the C_2-projection shows an inward centered view of a single staple-motif unit, *i.e.* the collinear X–Au–X (green–yellow–green) anchored by two surface Au atoms (navy-blue). To discern the two rotation angles, note that the blue rhombus displaces slightly clockwise with respect to the orange sub-structure while the staple vector (X–Au–X) rotates much further.[28] Right: side view of a C_2-section marked to indicate the special surface bonding and internal packing arrangements. Proceeding left to right (inside-outward), the sites are from the inner 12-Au (red pair), the inner 30-Au (orange quintet), the outer 12-Au (red pair), the 60-Au (blue quartet), and the 60-X sites (green pair) plus the outer 30-Au (yellow singlet). The collinear green–blue–orange alignment is evident at top and bottom, and forms the bold radial elements in Fig. 4.

the closed electronic shells, $3S^2$ and $2D^{10}$, respectively, depicted in Fig. 2 (inset). In the latter [4+] state, the HOMO–LUMO gap, separating the filled 2D orbitals from the empty 3S and the unoccupied portion of the 1H set, approaches 0.5 eV (see Fig. S6 (ESI†) for other charge states). The enhanced symmetry is also reflected in the restored degeneracy of the frontier orbitals *vs.* ref. 13 or 17 (Tables S1 and S2, ESI†).

The neutral [z = 0] form is destabilized by the partial (1/5) occupancy of a 5-fold degenerate level, indicating a Jahn–Teller mechanism, as suggested by Tofanelli and Ackerson to explain the observed charge-dependent thermal stability.[18] Spin-polarized calculations of the optimized neutral confirm a paired (spin-zero) rather than aligned (spin-unity) electronic configuration. Of course, it is already well established how the Jahn–Teller mechanism operates in icosahedral (I_h) symmetry systems such as the fullerides (C_{60} anions).[19]

Crucially, the finding that electronic closed-shell forms of I-$Au_{144}Cl_{60}^{[z]}$, hold the full I-symmetry agrees with the recent demonstration of the 60-fold equivalence of the thiolate ligands by NMR spectroscopy.[14]

Next, the halide-for-thiolate substitution[6] facilitates the description by eliminating both the conformationally variable R-groups and the pyramidal inversion mode of the bridging thiolate S-atom.[3]

The structure comprises 204 atomic sites, distributed over two sets each of {12, 30, 60}-fold equivalent sites.

Proceeding from the center outward, one finds concentric shells of {12, 30, 12; 60; 30, 60X} sites, where X denotes the shell of halide (X^-) sites, as color-coded in Fig. 1.

Because the respective shells must be aligned to preserve overall I-symmetry, eight (8) parameters suffice to specify completely the location of all 204 atoms.[20–22] A convenient choice includes the radii of the six shells along with two angles specifying the degree of rotation of the two 60-fold shells away from an I_h-symmetric configuration, *i.e.* these angles would vanish if I_h-symmetry held. For the optimized $Au_{144}Cl_{60}^{[2+]}$ compound, the six radial distances are {2.68, 4.89, 5.74, 7.02, 8.88 and 9.31 Å}, and the angles measure ~6 and ~17 degrees, as compared to the maximum rotation (~19 degrees).[20–21]

These values establish the extreme compactness of the optimized I-symmetry structure, based on the known 'staple-motif' units, compared against attractive alternatives, *e.g.* a Mackay-icosahedral I_h-(147,60) structure of metallic radius >10.0 Å, wherein the 60Au sub-shell assumes an open truncated-icosahedron (buckyball) form and the 60X bridging ligands are exterior, *i.e.* non-stapling.

The layer-by-layer (concentric-shell) construction in Fig. 1 gives a global picture of the structure and bonding, explicable largely *via* 'atom-packing' considerations.

The I-symmetry also simplifies the analysis of the local bonding characteristics: the three sections in Fig. 3 are selected as orthogonal projections,[20] presenting distinct views along one each from the many equivalent C_2, C_3, or C_5 axes.

From the C_2-projection, which features one complete staple-motif unit, the meaning of the two angles, one for each of the 60Au and the 60X shells, becomes apparent: the first angle transforms the blue squares into diamonds, while the second provides additional rotation of the green-yellow X–Au–X vectors needed to distribute uniformly the (nonbonding) X-sites.

From the C_3, or C_5 projections, one perceives how these displacements optimize the spatial distribution of the X-sites. The X–X distances are ~4.7 Å (across a C_2 axis, *via* an Au 'adatom' site), ~5.0 Å (around a C_3 axis), and ~4.0 Å (around a C_5 axis), as compared to the atomic dimension, ~3.6 Å (chloride ionic diameter).

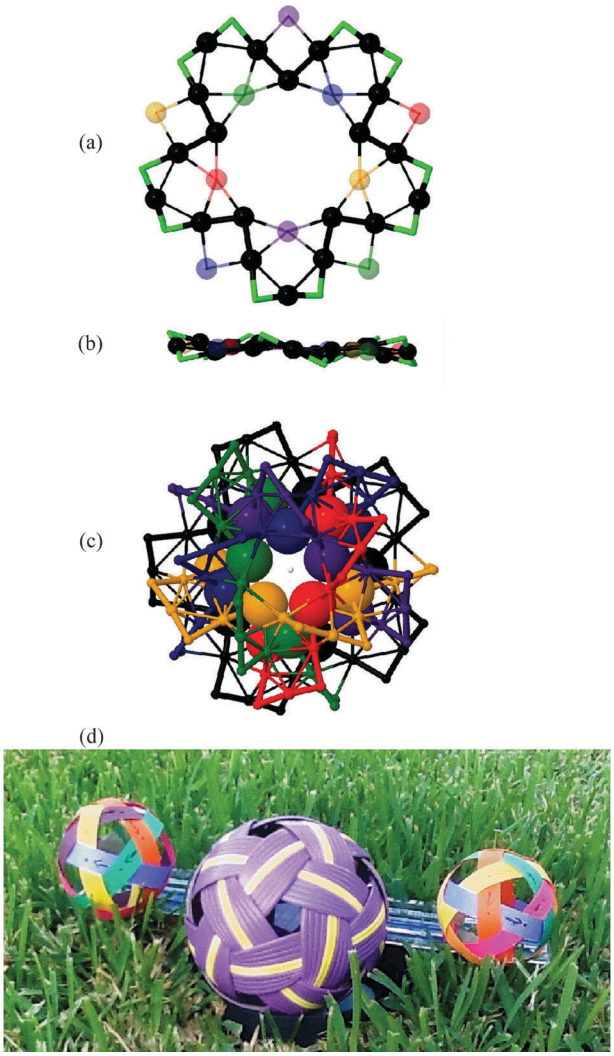

Fig. 4 Selected characteristics of I-$Au_{144}Cl_{60}^{[2+]}$. (a) A single strand (black) is identified by continuation of the radial elements identified in Fig. 3 (right). The black circles and green elbows constitute a single closed loop. Thick connecting lines designate the short bonds; the five (5) sets of distinctly coloured spheres mark under- and over-crossings of the other five strands. (b) In side-view, the structure is essentially flat, incorporating the two coplanar regular decagons from the 30-Au shells (Fig. 1, in orange), the 10 nearly coplanar sites from the 60-Au shell (blue in Fig. 1), and the zig–zag pattern of the 60-X sites (10 lime-green elbows) (c) hemisphere view of all six (6) coloured strands, obtained by elaboration from the single strand. All but 24 sites (the two 12-Au shells) of the 204 sites are incorporated into the weave structure. (d) Photograph of a standard woven kickball (*Sepak Tetraw* in the Thai language) on Texas Grass. It displays the same 6-strand network topology, including chirality, as that identified herein for the I-$Au_{144}X_{60}$ structure, thus serving an aide memorandum to the entire structure.[23]

Fig. 4(a) presents selected details of the local bonding arrangement. One familiar aspect[4] of the staple motif is the shorter (2.36 Å), stronger X–Au bonding parallel (tangential) to the cluster surface, as compared to the longer X–Au bonds (2.53 Å) perpendicular (radially directed). These are the shortest bonds in the entire structure.[23]

An unexpected aspect is revealed by continuation inward along these radial X–Au directions, which point toward Au-atoms of the inner 30 Au shell (orange). In fact, the 60 Au–Au equivalent contacts identified in this way are the shortest inter-Au distances ($\sim$2.77 Å) in the structure, including the compact 'inner core', *cf.* Fig. S2 (ESI†).

The bonding network identified by considering only these shortest X–Au and Au–Au bonds is presented in the Fig. 4(b and c), which forms a segmented great circle comprising five (5) staple-motif units. This provides a convenient way to visualize the entire structure (minus two sets of 12 Au atoms). It consists of six (6) equivalent 'strands' interwoven in the manner of the Thai woven kickball (Sepak Tatraw), depicted in Fig. 4(d).[23] The six-strand weave incorporates 180 of the 204 sites (Fig. S7, ESI†).

The optimized structure in [2+] and [4+] charge states is predicted to hold the exact *I*-symmetry, which greatly simplifies the analysis of the structure and bonding.

Both the compactness and the estimated cohesion with respect to prior stable units support the mechanical stability of the compound, regardless of the electronic configuration.

The gold-subhalide compound may appear an improbable candidate for chemical synthesis, given likely poor solubility in conventional solvents,[24] yet there exist many reports of so-called 'ligand-free' gold clusters, of dimension similar to this one ($\sim$1.8 nm diameter), obtained in complex media (ionic liquids, dendrimers *etc.*) incorporating halide or pseudo-halide agents.[25–27]

Conclusions

In summary, we have considered the crucial structural characteristics underlying the ubiquity of the $Au_{144}(SR)_{60}$ compounds (Faradaurates), employing isoelectronic substitution of thiolate anion by halide (chloride).

This allows one to establish theoretically the closed-shell electronic character of the [2+,4+]-charge-states, the latter in agreement with new results from electrospray ionization mass spectrometry.

One should therefore extend the isoelectronic method to other halides and charge-states, at least to [8−], that may be appropriate to those conditions, and to search for gold-subhalides $Au_{144}X_{60}^{[z]}$ in electrospray ionization mass spectra measured on complex-media samples.

Although no $Au_{144}(SR)_{60}^{[z]}$ compound has yielded to total structure determination, it is encouraging that the established structure[4] of $Au_{102}(SR)_{44}^{[0]}$ exhibits similar stereochemistry in its polar regions (comprising 30 of 44 thiolate groups) that may be explicable in terms of the simpler structure of the isoelectronic analog $Au_{144}X_{60}$.[29]

Finally, we stress the conceptual and theoretical advantages to employing the high *I*-symmetry whenever practicable: the large order of this group, O(60), implies a repeat unit of merely $Au_{12/5}X_1$ (3 2/5 atoms), fewer even than the $Au_2X_{3/2}$ (3 1/2 atoms) of the most studied small cluster, T_h-$Au_{24}X_{18}$ cluster, a group of O(12). This symmetry advantage is maintained, when replacing halogen (X) by thiolate (–SR) groups. The enormous reduction in complexity may facilitate a correlation among the structure, bonding, and electronic properties of ligand-protected noble-metal clusters, in the crucial size-range where the characteristically 'metallic' properties emerge, including the realistic computation of the capacitance[29] and the incipient plasmonic response,[30] in molecularly defined clusters.[31]

All details of experimental & computational methods and results are in the ESI.†

Acknowledgements

The authors gratefully acknowledge the contribution of Mr Nabraj Bhattarai who prepared and characterized (as described in ref. 13) the sample used in the ESI-MS measurements; discussions with Dr Michael Walter regarding gold subchlorides in ionic liquids; and the following funding sources: National Center for Research Resources (5 G12RR013646-12) and the National Institute on Minority Health and Health Disparities (G12MD007591) from the National Institutes of Health, and National Science Foundation (NSF) for support with grants DMR-1103730, ''Alloys at the Nanoscale: The Case of Nanoparticles Second Phase and PREM: NSF PREM Grant # DMR 0934218; ''Oxide and Metal Nanoparticles – The Interface Between Life Sciences and Physical Sciences''. All calculations were done in the Texas Advance Computing Center and by using resources of the Computational Biology Initiative. A.T.-F. acknowledges the support by CONACyT-Mexico.

Notes and references

1 J. C. Love, L. A. Estroff, J. K. Kriebel, R. G. Nuzzo and G. Whitesides, *Chem. Rev.*, 2005, **105**, 1103–1169.
2 M.-C. Daniel and D. Astruc, *Chem. Rev.*, 2004, **104**, 293–346.
3 I. G. Dance, *Polyhedron*, 1986, **5**, 1037–1104.
4 P. D. Jadzinsky, G. Calero, C. J. Ackerson, D. A. Bushnell and R. D. Kornberg, *Science*, 2007, **318**, 430–433.
5 P. Maksymovych, O. Voznyy, D. B. Dougherty, D. C. Sorescu and J. T. Yates Jr, *Prog. Surf. Sci.*, 2010, **85**, 206–240.
6 D.-E. Jiang and M. Walter, *Nanoscale*, 2012, **4**, 4234–4239.
7 A. Dass, *J. Am. Chem. Soc.*, 2011, **133**, 19259–19261.
8 M. Faraday, *Philos. Trans. R. Soc. London*, 1857, **147**, 145–180. G. Schatz (Northwestern Univ.) has proposed similarly that Faraday Band may denote the localized surface-plasmon resonance that emerges in protected larger clusters of gold (and other metals). Quotation repeated with permission of Prof. George Schatz.
9 N. K. Chaki, Y. Negishi, H. Tsunoyama, Y. Shichibu and T. Tsukuda, *J. Am. Chem. Soc.*, 2008, **130**, 8608–8610.
10 H. Qian and R. Jin, *Nano Lett.*, 2009, **9**, 4083–4087.

11 C. A. Fields-Zinna, R. Sardar, C. A. Beasley and R. W. Murray, *J. Am. Chem. Soc.*, 2009, **131**, 16266–16271.
12 C. Kumara and A. Dass, *Nanoscale*, 2011, **3**, 3064–3067.
13 D. Bahena, N. Bhattarai, U. Santiago, A. Tlahuice, A. Ponce, S. B. H. Bach, B. Yoon, R. L. Whetten, U. Landman and M. J. Jose-Yacamán, *J. Phys. Chem. Lett.*, 2013, **4**, 975–981.
14 O. A. Wong, C. L. Heinecke, A. R. Simone, R. L. Whetten and C. J. Ackerson, *Nanoscale*, 2012, **4**, 4099–4102.
15 N. T. Tran, D. R. Powell and L. F. Dahl, *Angew. Chem., Int. Ed.*, 2000, **39**, 4121–4125.
16 A. J. Karttunen, M. Linnolahti, T. A. Pakkanen and P. Pyykkö, *Chem. Commun.*, 2008, 465–467.
17 O. Lopez-Acevedo, J. Akola, R. L. Whetten, H. Grönbeck and H. Häkkinen, *J. Phys. Chem. C*, 2009, **113**, 5035–5038.
18 M. A. Tofanelli and C. J. Ackerson, *J. Am. Chem. Soc.*, 2012, **134**, 16937–16940.
19 C. C. Chancey and M. C. O'Brien, *The Jahn-Teller Effect in C60 and Other Icosahedral Complexes*, Princeton University Press, 1997, ch. 2 & 3.
20 R. Williams, *The Geometrical Foundation of Natural Structure: A Source Book of Design*, Dover Publications, 1979.
21 T. P. Martin, *Phys. Rep.*, 1996, **273**, 199–241.
22 A. L. Mackay, *Acta Crystallogr.*, 1962, **15**, 916–918.
23 Y. Nishiyama, *Int. J. Pure Appl. Math.*, 2012, **79**, 281–291.
24 J. Hartig, A. Stösser, P. Hauser and H.-G. Schnöckel, *Angew. Chem., Int. Ed.*, 2007, **46**, 1658.
25 D. F. Yancey, S. T. Chill, L. Zhang, A. I. Frenkel, G. Henkelman and R. M. Crooks, *Chem. Sci.*, 2013, **4**, 2912–2921.
26 Ch. Vollmer and Ch. Janiak, *Coord. Chem. Rev.*, 2011, **255**, 2039–2057; particularly Table 3 (p. 2046) & related discussion.
27 M. Walter, J. Akola, O. Lopez-Acevedo, P. D. Jadzinsky, G. Calero, C. J. Ackerson, R. L. Whetten, H. Grönbeck and H. Häkkinen, *Proc. Natl. Acad. Sci. U. S. A.*, 2008, **105**, 9157.
28 D. Bochicchio and R. Ferrando, *Nano Lett.*, 2010, **10**, 4211–4216.
29 A. Held, M. Moseler and M. Walter, *Phys. Rev. B: Condens. Matter Mater. Phys.*, 2013, **87**, 045411 and reference therein.
30 X. Lopez-Lozano, C. Mottet and H.-Ch. Weissker, *J. Phys. Chem. C*, 2013, **117**, 3062–3068.
31 L. Cademartiri and V. Kitaev, *Nanoscale*, 2011, **3**, 3435–3446.